Dye−Exchange Dynamics in Micellar Solutions Studied by Fluorescence Correlation Spectroscopy

ARTICLE *in* THE JOURNAL OF PHYSICAL CHEMISTRY B · MAY 2007

Impact Factor: 3.3 · DOI: 10.1021/jp0657639 · Source: PubMed

4 AUTHORS:

Mercedes Novo
University of Santiago de Compostela
60 PUBLICATIONS **646** CITATIONS
SEE PROFILE

Suren Felekyan
Heinrich-Heine-Universität Düsseldorf
51 PUBLICATIONS **1,688** CITATIONS
SEE PROFILE

Claus A M Seidel
Heinrich-Heine-Universität Düsseldorf
133 PUBLICATIONS **5,737** CITATIONS
SEE PROFILE

Wajih Al-Soufi
University of Santiago de Compostela
74 PUBLICATIONS **744** CITATIONS
SEE PROFILE

Dye-Exchange Dynamics in Micellar Solutions Studied by Fluorescence Correlation Spectroscopy

Mercedes Novo,*,† Suren Felekyan,‡ Claus A. M. Seidel,‡ and Wajih Al-Soufi†

Departamento de Química Física, Facultade de Ciencias, Universidade de Santiago de Compostela, E-27002 Lugo, Spain, and Lehrstuhl für Molekulare Physikalische Chemie, Heinrich-Heine Universität Düsseldorf, Universitätsstrasse 1, D-40225 Düsseldorf, Germany

Received: September 5, 2006; In Final Form: January 15, 2007

We investigated the dye-exchange dynamics between rhodamine 123 (R123), a mitochondrial fluorescent dye, and micelles as membrane mimetic systems. In the presence of neutral micelles (Triton X-100 and Brij 35) R123 partitions between the aqueous solution and the micellar pseudo-phase, undergoing red shift of the absorption and the emission spectra. Fluorescence correlation spectroscopy (FCS) was used to study the dynamics of these systems over an extremely wide time range and at the single-molecule level, yielding information in one and the same experiment about the diffusional dynamics of free and bound rhodamine and about the dye-exchange dynamics as well as several photophysical properties of the rhodamine bound to the micelles. It was found that the entry rate constants are diffusion-controlled, indicating that there are no geometric or orientational requirements for the association of the dye with the micelle. With respect to the dye-exchange dynamics, micelles are found to behave as soft supramolecular cages in contrast to other rigid supramolecular cavities, such as cyclodextrins. The exit rate constants depend on the surfactant and determine the stability of the binding. Single-molecule multiparameter fluorescence detection (MFD) was used to examine the fluorescence properties of individual molecules in comparison to ensembles of molecules. The MFD histograms confirm the fast dye-exchange dynamics observed by FCS and yield mean values of fluorescence lifetimes and anisotropies in agreement with those obtained in bulk measurements.

Introduction

The exchange dynamics through biological membranes is an essential point to understand the transfer of matter in living systems. Moreover, the action mechanisms of drugs are very much determined by both their entry rates into the cell membranes and their exit rates, which control the time scale of binding and the rate of release of the drug. In this work we present a new approach to study this exchange dynamics by means of fluorescence correlation spectroscopy (FCS), using micelles as membrane mimetic systems and a typical mitochondrial fluorescence marker, rhodamine 123 (R123), as a probe. Like membranes, micelles are highly cooperative, dynamic, organized molecular assemblies, where hydrophobic interactions play an important role. As model systems they are simpler, with well-defined sizes and advantageous optical properties.[1]

Micelles can also be considered as soft supercages in which host molecules can enter yielding supramolecular complexes, for which the association/dissociation dynamics are of critical importance.[2] We have recently used FCS to study the association dynamics of host−guest supramolecular complexes formed by cyclodextrins, which provide more rigid and smaller cavities as compared to micelles.[3] There we found that the association rate constant is limited by geometrical and orientational requirements between host and guest, whereas the dissociation rate is mainly determined by specific host−guest interactions. It is also the purpose of this work to compare the dynamics of these two types of supramolecular systems, which have important structural differences but the same kind of hydrophobic forces involved in complex formation.

So far, most of the information about the exchange dynamics of solute molecules between the micellar pseudo-phase and the aqueous solution has been obtained by fluorescence quenching experiments.[4,5] This method usually involves a fluorescent probe with high affinity to the micellar pseudo-phase whose fluorescence is quenched by the presence of a second molecule or ion (quencher). The exchange dynamics of the quencher between the micellar and the aqueous phases can be resolved from steady-state and time-resolved fluorescence measurements with varying quencher concentrations. An inconvenience of the method is that only certain quenchers are adequate for the fluorescence probe and the micellar system used. Phosphorescence experiments have also been used to study the exchange dynamics in micelles, but they are limited to certain suitable probes and low entry/exit rates.[4]

In a previous work we demonstrated the advantages of FCS to determine the association/dissociation rate constants of fluorescent dyes with cyclodextrins.[3] FCS is a fluctuation correlation method that allows one to measure the dynamics of molecular processes from the small changes in molecular concentration or chemical states that arise from spontaneous fluctuations around equilibrium. Therefore FCS yields direct information about the dynamics of the fluorescent probe without the need for external disturbances or quencher molecules. Recent developments of this technique allow us to register full correlation curves of an extremely wide dynamic range from picoseconds to seconds,[6] making it possible to study all dynamic and photophysical processes that take place in that wide time

* Author to whom correspondence should be addressed. Phone: +(34) 982 285871. Fax: +(34) 982 285872. E-mail: mnovo@lugo.usc.es.
† Universidade de Santiago de Compostela.
‡ Heinrich-Heine Universität Düsseldorf.

10.1021/jp0657639 CCC: $37.00
Published on Web 03/17/2007

scale in one and the same experiment. These processes are, from fast to slow times, the excitation−deactivation of the fluorophore, the chemical reactions involving the fluorophore and its conversion to the triplet state, and the diffusional dynamics of the fluorophore. Another important feature of FCS is that it extends the measurement of dynamic processes down to the single-molecule level by using very small sample volumes determined by a confocal setup and nanomolar fluorophore concentrations. At this level another powerful technique has been developed, the single-molecule multiparameter fluorescence detection (MFD), which involves the simultaneous and independent determination of several fluorescence parameters (intensity, lifetime, and anisotropy) for each individual molecule observed.[7−9] In this work we have also applied this technique to compare the photophysical parameters of the system at the single-molecule level with those obtained by classical fluorescence techniques in bulk measurements.

Few articles have been published using FCS for the study of micellar systems.[10−14] All of them focused on the determination of typical properties of the micelles, such as the critical micellar concentration (CMC) and the mean aggregation number (N_{ag}), which can be obtained from the analysis of the diffusional part of the correlation curves (microseconds to seconds time range). Most of the reported studies use fluorescence probes with amphiphilic properties, which have very high affinity to the micellar pseudo-phase but may significantly influence the properties of the micelles.[11−13] Very recently a study with noncovalently bound dye molecules and surfactants with different charges has been published, where the determination of the CMC by means of FCS is discussed.[14] In systems where charged dyes bind strongly to oppositely charged ionic surfactants these authors found at the CMC a sharp transition in the diffusion times determined from correlation curves measured below and above the CMC.

In this work we use two neutral surfactants, Triton X-100 (TX-100, *t*-Oct-C_6H_4-$(OCH_2CH_2)_{10}OH$, $M_w = 646.85$ g/mol), and Brij 35 ($C_{12}H_{25}(OCH_2CH_2)_{23}OH$, $M_w = 1198$ g/mol). Both surfactants are formed by a polar poly(ethylene glycol) chain and a hydrophobic carbon chain, differing mainly in the length of the poly(ethylene glycol). These two surfactants have been extensively studied, so their properties regarding micelle formation are quite well established: CMC = 0.26 mM and $N_{ag} = 143$ for TX-100, CMC = 0.06 mM and $N_{ag} = 40$ for Brij 35.[4] Nevertheless, more precise, recent studies reported significant variations of the aggregation numbers depending on surfactant concentration and on temperature.[15−19] As a fluorescence probe the positively charged R123 was chosen due to its ability to partition between the micellar pseudo-phase and the aqueous solution and its high fluorescence quantum yield and photostability, properties which make it very suitable for FCS studies. To avoid the strong electrostatic effects controlling the association of this molecule with charged micelles,[20,21] neutral surfactants were selected, which allow investigation of the hydrophobic forces involved in the dye-exchange dynamics.

Experimental Section

Materials. Rhodamine 123 was purchased from Sigma-Aldrich and used as received. The surfactants TX-100 and Brij 35 (both Fluka BioChemika) were checked for fluorescence impurities and were found to be clean for classical fluorescence measurements and for FCS experiments. At the single-molecule detection (SMD) level TX-100 was not pure enough, but Brij 35 could be used although its fluorescence impurities represented approximately 6% of the total registered bursts at highest concentration used. Water was purified with a Milli-Q system.

Sample Preparation. Stock aqueous solutions of the surfactants were prepared at concentrations of 15−30 mM for TX-100 and 12−20 mM for Brij 35. Stock solutions of R123 were prepared with 10-fold higher concentrations than that adequate in each kind of titration (approximately 3×10^{-6} M in absorption, 10^{-6}−10^{-7} M in time-resolved and steady-state fluorescence, and 10^{-8}−10^{-9} M in FCS). Except for SMD experiments, the measuring samples were prepared by dilution of a constant volume of the corresponding R123 stock together with different volumes of the surfactant stock solution and addition of water to adjust to a certain total volume. The accuracy of these volumes was checked by weighing, and concentration corrections were made. SMD samples were prepared by dipping a pipet tip first into the R123 solution and then washing it in the measuring droplet of the surfactant solution.

Absorption and Fluorescence Measurements. Absorption spectra were recorded in a Varian-Cary 300 spectrometer using quartz cells with a path length of 10.0 mm. The baseline was recorded with water in both sample and reference cells. Both steady-state and time-resolved fluorescence measurements were performed with an Edinburgh Instruments F900 spectrofluorimeter, equipped with a 450W xenon lamp as an excitation source for steady-state measurements and a hydrogen-filled nanosecond flash lamp for lifetime measurements using the time-correlated single photon counting (TCSPC) technique. The typical pulse half-width of the flash lamp is 1.5 ns. Steady-state anisotropy measurements were carried out in a SPEX Fluorolog-2 FL-340 spectrofluorimeter with filter polarizers. Excitation wavelengths were 496 nm for steady-state emission spectra and 310 nm in time-resolved measurements. Fluorescence decays were measured at 525 nm. All experiments were carried out at 20 ± 1 °C.

FCS and MFD Measurements. The confocal epi-illuminated setup used for the FCS measurements has been described elsewhere.[3,6] The fluorescent samples were excited by a linearly polarized argon ion laser beam (Innova Sabre, Coherent, Palo Alto, CA, 496.5 nm continuous wave emission) focused into the sample by a microscope objective (Olympus 60, NA 1.20, water immersion). The fluorescence was collected by the same objective and then refocused onto a pinhole (diameter of 100 μm) in the image plane. The two polarization components were separated by a polarizing cube and then individually detected by avalanche photodiodes (MPD PDM-50, Bolzano, Italy). Two band-pass filters (HQ533/46, AHF Analysentechnik, Tübingen, Germany) in front of the detectors discriminated fluorescence from laser light scattered at the excitation wavelength and from Raman scattered light of the solvent molecules. Both output signals were processed and stored by modified TCSPC modules (SPC 132, Becker & Hickl GmbH, Berlin, Germany).[6] Correlation curves were calculated with a fast home-built routine that runs under LabVIEW (National Instruments).[6] Typically 128 million photons were collected for each correlation curve with count rates between 50 and 350 kHz. All measurements were made at room temperature, stabilized at 21 °C. The excitation power as measured in the focus of the microscope objective by a power meter (Coherent, Fieldmaster, model FM-2) was typically 62 μW, corresponding to a mean irradiance of $I_0/2 \approx 5.5$ kW/cm^2.[22]

The focal area and the detection volume have been calibrated with R110 in aqueous solutions at a low irradiance, D(R110, 25 °C) = $3.4 \pm 0.3 \times 10^{-10}$ m^2 s^{-1}, yielding a radial $1/e^2$ radius of $w_{xy} = 0.6$ μm and a sample volume of ~5 fL.[3] All diffusion coefficients are corrected for temperature and viscosity effects

and are given for 25 °C. All given uncertainties correspond to one standard deviation from the fits.

For MFD measurements the same setup was used as for FCS, but the Ar^+ laser was mode-locked to deliver pulsed excitation (496.5 nm, 73.5 MHz, 150 ps). R123 solutions were strongly diluted to ensure that only brief fluorescence bursts (~3 ms) are detected from single R123 molecules during their transit through the sample volume. The principles of MFD have been described in detail.[8,23] For each detected photon both the arrival time and the polarization with respect to the linear polarization of the excitation laser are recorded. These data are then used to calculate a mean fluorescence lifetime, τ, and the steady-state anisotropy, r, for each of the registered bursts.[24,25] The anisotropy was corrected for mixing of polarizations by the microscope objective and for slightly different detection efficiencies in the two detection channels.

Data Analysis. The series of absorption and emission spectra obtained in the titrations of R123 with each of the surfactants were analyzed using principal components global analysis (PCGA).[26] This method can be applied to a series of spectra that vary with an external parameter, as the micelle concentration in this case. The first step of PCGA is the principal components analysis (PCA), where the minimal number of spectral components responsible for the observed variations is obtained. This information helps to draw up a theoretical model that is used in the second step as fit function for a nonlinear least-squares global analysis using the whole spectra as a data set. The results of this global fit are the physicochemical parameters involved in the model and the individual spectra of the components.

Individual fits of fluorescence decays were performed with the software package from Edinburgh Instruments.

For FCS curves two levels of nonlinear data analysis have been applied: (1) Individual correlation curves were fitted by a fast home-built routine that runs under LabVIEW (National Instruments). (2) Series of correlation curves measured at different surfactant concentrations were analyzed by global "target" analysis programmed in OriginPro 7.0 (OriginLab Corporation) or in Matlab (The MathWorks).

Theory

Mechanism. Above the CMC surfactants aggregate in aqueous solution to form micelles (M) with a mean number of surfactants given by the mean aggregation number, $N_{ag.}$ Near the CMC micelles are generally spherical, and the concentration of nonaggregated surfactant molecules is equal to the CMC, so the concentration of micelles [M] can be obtained from the total surfactant concentration [S] as follows

$$[\mathrm{M}] = \frac{[S] - \mathrm{CMC}}{N_{\mathrm{ag}}} \tag{1}$$

(The values used in this work are CMC = 0.26 mM and N_{ag} = 143 for TX-100 and CMC = 0.06 mM and N_{ag} = 40 for Brij 35).[4]

When a dye is added to a surfactant solution above the CMC, it can either associate totally with the micellar pseudo-phase or it can partition between the aqueous solution and the micellar pseudo-phase. In the latter case a partition equilibrium model is considered between free dye (D_f) and dye bound to the micelles (D_b)

$$\mathrm{D_f} + \mathrm{M} \overset{K}{\rightleftharpoons} \mathrm{D_b} \tag{2}$$

where K is the equilibrium binding constant.[4] As for any other equilibrium process, absorption and fluorescence titrations with constant concentrations of dye and varying concentrations of micelles (i.e., surfactant) allow for the determination of the binding constant. Considering changes of brightness (Table 1 and Figure 2), one can only detect micelle binding sites, which change the dye properties in a characteristic manner. However, the analysis of the dye's diffusion properties by FCS will detect all bound dye species. Please note that the different properties need not yield necessarily the same results for a heterogeneous system.

FCS. FCS analyzes spontaneous fluorescence intensity fluctuations that may be caused by various processes at the molecular level: changes in concentration of a fluorophore or due to translational motion in and out of the sample volume, changes in the excited singlet or triplet state population, or changes in the physicochemical properties of the system, for example, due to a chemical reaction or association. The normalized autocorrelation function $G(\tau)$ of the intensity fluctuations $\delta F(t) = F(t) - \langle F \rangle$ indicates in this case the variation in the probability to register from the same molecule a second photon at the correlation time τ, once a first was emitted

$$G(\tau) = \frac{\langle \delta F(t) \cdot \delta F(t+\tau) \rangle}{\langle F(t) \rangle^2} \tag{3}$$

Relating $G(\tau)$ to the intensity fluctuations $\delta F(t)$ eliminates the usual time invariant term $\langle F(t) \rangle^2 / \langle F(t) \rangle^2 = 1$ in eq 3. This constant term is directly subtracted from the experimental correlation curves.

The time-dependent parts of the correlation function for translational diffusion G_D, triplet-state formation G_T, and antibunching G_F are given by[27−29]

$$G_{\mathrm{D}}(\tau) = \frac{1}{N}\left(1 + \frac{\tau}{\tau_{\mathrm{D}}}\right)^{-1}\left(1 + \left(\frac{w_{xy}}{w_z}\right)^2 \frac{\tau}{\tau_{\mathrm{D}}}\right)^{-1/2} \tag{4}$$

$$G_{\mathrm{T}}(\tau) = (1 + A_{\mathrm{T}}\, \mathrm{e}^{-\tau/\tau_{\mathrm{T}}}) \qquad A_{\mathrm{T}} = \frac{T}{1-T} \tag{5}$$

$$G_{\mathrm{F}}(\tau) = (1 - A_{\mathrm{F}}\, \mathrm{e}^{-\tau/\tau_{F}}) \qquad A_{\mathrm{F}} = 1\text{-} \tag{6}$$

A three-dimensional Gaussian distribution of the detected fluorescence is assumed with radial and axial 1/e radii w_{xy} and w_z, respectively. N is the mean number of fluorescent molecules within the sample volume, and τ_D is the translational diffusion time of the molecules across the sample volume, which is related to the translational diffusion coefficient D by

$$D = \frac{{w_{xy}}^2}{4\tau_{\mathrm{D}}} \tag{7}$$

The time τ_T is determined by the triplet lifetime, and the amplitude A_T is related to the fraction of molecules, T, in the "dark" triplet state.

Under the condition $\tau_D \gg \tau_T \gg \tau_F$ the full correlation curve is given by the product of the individual functions from the eqs 4, 5, and 6

$$G(\tau) = G_{\mathrm{F}} \times G_{\mathrm{T}} \times G_{\mathrm{D}} \tag{8}$$

Correlation Function for the Partition Equilibrium. The correlation function taking into account the variation in the diffusion coefficient and in the brightness of a dye due to a chemical equilibrium reaction has been described previously.[3]

The partition equilibrium (eq 2) between free and bound dye is treated as a chemical reaction with (association) equilibrium constant K, association rate constant k_+, and dissociation rate constant k_-

$$K = \frac{k_+}{k_-} \tag{9}$$

Under conditions where the micelle concentration is always much higher than that of the dye, this concentration coincides with the initial micelle concentration $[M]_0$ ($[D_f] \ll [M] \approx [M]_0$), and the reaction is pseudo-first-order with the relaxation time τ_R given by

$$\tau_R = (k_+[M]_0 + k_-)^{-1} \tag{10}$$

Applying the assumption that the relaxation rate of the reaction is much faster than the typical diffusion times of free, τ_f, and bound dye, τ_b, (i.e., fast exchange, $\tau_R \ll \tau_f,\tau_b$), the following correlation function for the diffusion and equilibrium reaction is obtained

$$G_{DR}(\tau) = \frac{1}{N_f + N_b}\left(1 + \frac{\tau}{\bar{\tau}_D}\right)^{-1}\left(1 + \left(\frac{w_{xy}}{w_z}\right)^2 \frac{\tau}{\bar{\tau}_D}\right)^{-1/2}(1 + A_R\, e^{-\tau/\tau_R}) \tag{11}$$

where the diffusion term is defined by a mean diffusion time $\bar{\tau}_D$ and an amplitude that depends on the mean numbers N_f and N_b of free and bound dye in the sample volume. The reaction term has an amplitude A_R and a correlation time given by the relaxation time τ_R.

The mean diffusion time $\bar{\tau}_D$ depends on the individual diffusion coefficients D_f and D_b and on the fractions $X_x = N_x/(N_f + N_b)$

$$\bar{\tau}_D = \frac{{w_{xy}}^2}{4(X_f D_f + X_b D_b)} = (X_f(\tau_f)^{-1} + X_b(\tau_b)^{-1})^{-1} \tag{12}$$

The parameters τ_D, τ_R, and A_R can be expressed directly as function of $[M]_0$ and K.

$$\bar{\tau}_D = \frac{\tau_f(1 + K[M]_0)}{1 + \frac{\tau_f}{\tau_b}K[M]_0} \tag{13}$$

$$\tau_R = (k_-(1 + K[M]_0))^{-1} \tag{14}$$

$$A_R = \frac{N_f N_b (Q_f - Q_b)^2}{(Q_f N_f + Q_b N_b)^2} = \frac{K[M]_0(1 - Q)^2}{(1 + QK[M]_0)^2} \tag{15}$$

The reaction amplitude, A_R, depends on the brightness ratio $Q = Q_b/Q_f$ of free and bound guest. The species-dependent brightness is defined by the product of the extinction coefficients, fluorescence quantum yield, and detection efficiency $\epsilon_x \Phi_{(F)x} g_x$. The brightness ratio Q can be determined by integrating the pure spectra of free and bound guest in the wavelength interval determined by the emission filter used in FCS.

If the dye triplet population cannot be neglected and the complexation equilibrium relaxation is taken to be independent from antibunching and triplet state formation, then the complete correlation function is given by the product of the individual correlation functions given in eqs 5, 6, and 11

$$G(\tau) = G_F \times G_T \times G_{DR} \tag{16}$$

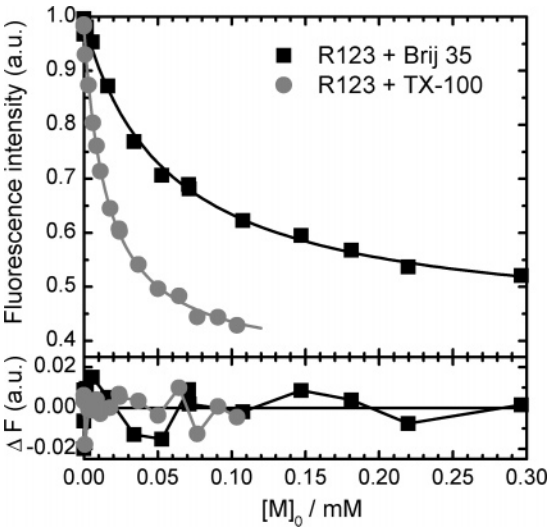

Figure 1. Fluorescence intensities of R123 at 525 nm versus micelle concentration for TX-100 (gray circles) and Brij 35 micelles (black squares). Symbols represent experimental data, and lines fitted curves of eq 17 with the parameters given in the text. The graph at the bottom shows the corresponding residual plots. λ_{exc} = 496 nm. Micelle concentrations were calculated using eq 1 and the values of CMC and N_{ag} given there.

Results and Discussion

Partition Equilibrium. Titration measurements were carried out by adding different concentrations of TX-100 or Brij 35 to a constant concentration of R123 in aqueous solution. Both absorption and fluorescence emission spectra of R123 showed no changes after addition of surfactant at concentrations smaller than the corresponding CMC values. On the contrary, at higher surfactant concentrations, spectral variations were observed: The absorption spectrum shifted to the red with a well-defined isosbestic point, and the emission spectrum showed also a red shift and a significant decrease in intensity. Figure 1 shows the variations of the fluorescence intensity of R123 as a function of the concentration of micelles for the two surfactants under study. The dependence observed is typical for an association equilibrium between two species.

All of these experimental findings support a partition equilibrium of the dye between the aqueous solution and the micellar pseudo-phase with an equilibrium binding constant K (eq 2). Under the experimental conditions used (fixed dye concentration and an excess of micelles compared to the total dye concentration) and in the absence of excited-state association/dissociation processes, the following relation can be deduced between the fluorescence intensity (or the absorbance) at a certain wavelength, $F(\lambda)$, and the concentration of micelles

$$F(\lambda) = \frac{F_f(\lambda) + F_b(\lambda)K[M]_0}{1 + K[M]_0} \tag{17}$$

where $F_f(\lambda)$ and $F_b(\lambda)$ are the limiting fluorescence intensities (or absorbances) at wavelength λ of the dye free in the aqueous solution and bound to the micelles, respectively. The same equation can be applied to other properties that depend linearly on the molar fractions of the free or bound dye.

The nonlinear least-squares fits of this equation to the experimental data were very satisfactory, as shown in Figure 1

TABLE 1: Binding Equilibrium Constants of R123 with TX-100 and Brij 35 Micelles and Photophysical Parameters of R123 in Aqueous Solution and Bound to the Micelles

	R123 in water	R123 bound to TX−100 micelles	R123 bound to Brij 35 micelles
$K/10^3$ M^{-1}		65 ± 3	19 ± 1
ϕ_β/ϕ_ϕ [a]	1	0.74	1.02
Q_b/Q_f [b]	1	0.42	0.55
r [c]	0.006 ± 0.003	0.137 ± 0.004	0.093 ± 0.004
t/ns (%B_b) [d]	$t_f = 4.01 \pm 0.01$	$t_{b1} = 2.7 \pm 0.2$ (90%) $t_{b2} = 0.5 \pm 0.2$ (10%)	$t_{b1} = 4.7 \pm 0.3$ (92%) $t_{b2} = 0.8 \pm 0.3$ (8%)

[a] Fluorescence quantum yield of bound R123 relative to free R123 (estimated error of 5%). [b] Brightness ratio under conditions of FCS measurements, i.e., $\lambda_{exc} = 496$ nm (estimated error of 5%). [c] Steady-state anisotropy. [d] Fluorescence lifetimes with its percentage contribution to total fluorescence at 525 nm with excitation at 310 nm. The lifetimes of bound dye were determined from fits of a sum of three exponentials $F(t) = B_f \exp(-t_f/t) + B_{b1} \exp(-t_{b1}/t) + B_{b2} \exp(-t_{b2}/t)$, and the corresponding percentage contributions were calculated as $B_{b1}/(B_{b1} + B_{b2})$ and $B_{b2}/(B_{b1} + B_{b2})$. The reduced χ^2 values were always below 1.2.

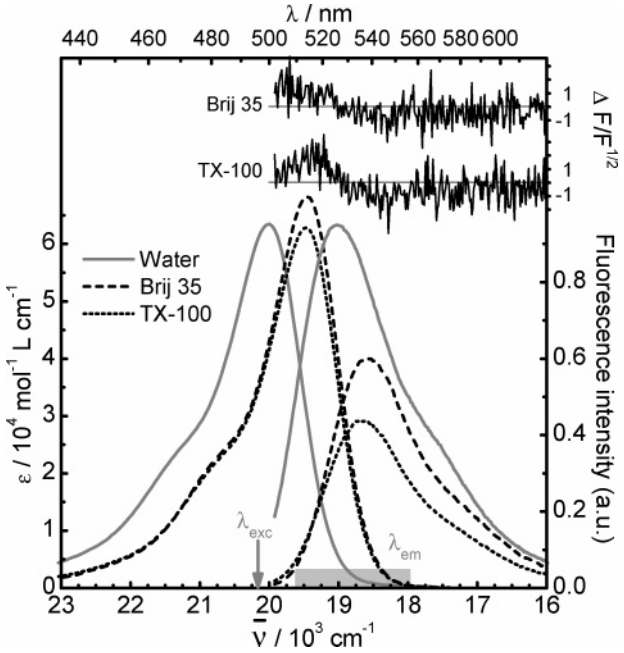

Figure 2. "Pure" absorption and fluorescence emission spectra of R123 in aqueous solution (gray solid lines), R123 bound to Brij 35 micelles (black dashed lines), and R123 bound to TX-100 micelles (black dotted lines) as obtained from principal component global analysis of eq 17 to the titration data shown in Figure 1. In the upper part examples of the weighted residual spectra ($\Delta F/F^{1/2}$) are shown for the fits to the fluorescence spectra at $[M]_0 = 0.1$ mM. Also indicated are the excitation wavelength ($\lambda_{exc} = 496$ nm) and the range of emission wavelength detected (λ_{em}) in the FCS measurements as determined by the band-pass filters used.

for the fluorescence intensities of R123 at a single wavelength (525 nm) in the presence of TX-100 and Brij 35 micelles. Global nonlinear fits using PCGA to the full spectra yield more precise values of the equilibrium binding constants as well as the pure spectra of the two species involved, i.e., free dye and dye bound to the micelles. The mean values of the equilibrium binding constants obtained from absorption and fluorescence titrations are given in Table 1. Figure 2 shows the absorption and fluorescence emission spectra of R123 in aqueous solution and bound to the micelles of TX-100 and Brij 35. The absorption spectra of R123 in the two types of micelles are nearly identical, with the same red shift with respect to the spectrum in water. Emission spectra are very similar, with the intensity decrease larger in TX-100 micelles than that in Brij 35 micelles, whereas the latter cause a somewhat stronger red shift.

The ratio between the fluorescence intensities of free and bound R123 (brightness ratio $Q = Q_b/Q_f$) that will be observed in FCS measurements with a given excitation wavelength can be determined by integrating the corresponding pure fluorescence emission spectra (Figure 2) within the limits of the emission filters used (gray bar in Figure 2). The relative quantum yields ϕ_b/ϕ_f are calculated from the same spectra but integrating the full spectral range and correcting for the different molar absorption coefficients of the species at the excitation wavelength. The results are given in Table 1. The pure emission spectra in Figure 2 seem to indicate a great decrease of the fluorescence quantum yield of R123 bound to the micelles with respect to free dye, but it must be noted that a significant part of the decrease in fluorescence is due to the lower absorption of bound R123 at the excitation wavelength (496 nm) induced by the strong spectral shift of the absorption spectra upon binding. If this difference in absorption is taken into account, then the decrease of the fluorescence quantum yield of R123 when binding to the TX-100 micelles is only approximately 25%, whereas no change or even a small increase of fluorescence quantum yield is found in Brij 35 micelles (see relative quantum yields in Table 1). Thus, using an excitation wavelength of 496 nm, the difference in the brightnesses of free and bound R123 is mostly determined by the spectral shift of the R123 absorption spectrum, leading to very different molar absorption coefficients at the excitation wavelength, as shown in Figure 2. This way, even if there is no fluorescence quenching, the entry/exit processes of R123 into/out of a micelle result in an effective variation ("blinking") of the brightness, which can be observed in FCS measurements.

Time Correlated Single Photon Counting. To determine the fluorescence lifetimes of R123 bound to the micelles, fluorescence decays were measured at 525 nm for different surfactant concentrations. In the absence of surfactant and at concentrations below the CMC, single-exponential decays are obtained with the lifetime of R123 in water (Table 1). At surfactant concentrations above the CMC, the fluorescence decays can be satisfactorily fitted with two exponentials, but the corresponding lifetimes vary with the surfactant concentration. This indicates that each of the two lifetimes does not correspond to a single species, but the lifetimes are average times of more than two species. Taking into account that, at the surfactant concentrations used, a certain proportion of free R123 is always present together with bound R123, fits with a three-exponential function (see footnote d of Table 1) were performed using a fixed lifetime of 4.0 ns, representing free R123. Then the remaining two fitted lifetimes coincide within error at all surfactant concentrations and show increasing amplitudes as this concentration is increased, indicating that they are due to bound R123. The longer lifetime must be assigned to the lifetime of R123 bound to the micelles, since its contribution is approximately 90% of the total fluorescence of this species. In the case of TX-100 micelles, this lifetime of bound R123 is shorter than that of free R123, as could be expected from the observed decrease of the fluorescence quantum yield (Table 1). On the contrary, the R123 bound to Brij 35 micelles shows a slightly longer lifetime than free R123, in agreement with the somewhat higher quantum yield. To explain the appearance of a second, short lifetime for bound R123, fluorescence decays were measured at different emission wavelengths with samples of high surfactant concentrations. It was found that the contribu-

tion of the short lifetime decreases when increasing the emission wavelength, suggesting that the short lifetime reflects the solvation dynamics of R123 inside the micelles. Such relaxation processes inside organized structures such as micelles show time constants of some hundreds of picoseconds, as reported in the literature.[30] This hypothesis needs to be studied further with lifetime measurements of higher time resolutions. Due to the lower sensitivity of the TCSPC setup much higher R123 concentrations had to be used than those in single-molecule spectroscopy. Thus, the small amount of impurities in the surfactants found at the single-molecule level (see below) plays no role in these bulk lifetime measurements.

Fluorescence Anisotropy. The effect of micelle binding in the steady-state anisotropy of R123 was also studied by fluorescence titrations under polarized excitation and emission. In the absence and at surfactant concentrations lower than the CMC, the same anisotropy was obtained, which was very close to zero (Table 1). This indicates that the presence of surfactant monomers has no influence on the rotational motion of the rhodamine, which is completely free to rotate as in water. At surfactant concentrations above the CMC, a systematic increase of R123 anisotropy is observed for both TX-100 and Brij 35 micelles. Taking into account that each sample is a mixture of free and bound R123, the observed anisotropy ($r(\lambda)$) is an average of the anisotropies of the two species ($r_f(\lambda)$ for free R123 and $r_b(\lambda)$ for bound R123), weighted by their fluorescence intensities

$$r(\lambda) = \frac{r_f(\lambda) + r_b(\lambda)\dfrac{F_b(\lambda)}{F_f(\lambda)}K[M]_0}{1 + \dfrac{F_b(\lambda)}{F_f(\lambda)}K[M]_0} \qquad (18)$$

Using the known fluorescence intensities of the two species, this equation can be satisfactorily fitted to the anisotropy values determined at a certain wavelength yielding the anisotropies of free and bound R123 and the binding constant (data are not shown). Nevertheless, to use the whole spectral information, each series of polarized emission spectra, separated for vertical and horizontal polarization, were globally fitted using eq 17, and from the results the anisotropies of free and bound R123 were calculated. The fits were very good, yielding values of the binding equilibrium constants that are in perfect agreement with those obtained in the absorption and fluorescence titrations. Mean values of the anisotropies of each species are given in Table 1. The anisotropy of free R123 coincides with that obtained directly from pure R123 solutions. The values obtained for the anisotropies of bound R123 are significantly larger than the anisotropy of free R123, indicating that the rotation of the rhodamine is hindered inside the micelles. The anisotropy of R123 bound to TX-100 micelles is significantly larger than that of R123 bound to Brij 35 micelles, but this may be due to the shorter fluorescence lifetime of the former species (Table 1). To compare the anisotropy results in the two types of micelles, the corresponding rotational correlation times are calculated using Perrin's equation $r = r_0/(1 + \tau/\rho)$ with the values given in Table 1 and a limiting anisotropy of $r_0 = 0.373$ reported for xanthene dyes.[10] A value of $\rho = 1.6$ ns is obtained for the rotational correlation time of bound R123 in both types of micelles, much longer than that in water ($\rho = 0.06$ ns). This time coincides quite well with the reported rotational correlation times, reflecting the internal motion of other rhodamines in TX-100 micelles.[31,32] This suggests that fluorescence depolarization of bound R123 is mainly due to its internal motion inside the micelle, which presents similar hindrances in TX-100 and Brij 35 micelles.

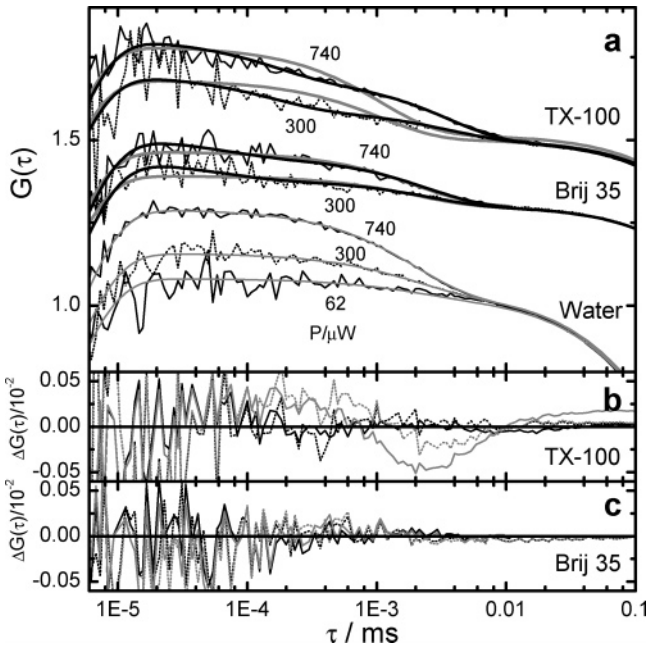

Figure 3. (a) Experimental correlation curves of R123 with varying excitation power. Lower group of lines: free R123 in water at 62 μW, 300 μW and 740 μW, from bottom to top. Middle group: R123 in 21 mM Brij 35 ([M] = 0.52 mM) solution at 300 μW (lower dotted curve) and 740 μW (upper solid curve). Upper group: R123 in 31 mM TX-100 ([M] = 0.21 mM) solution at 300 μW (lower dotted curve) and 740 μW (upper solid curve). Gray heavy lines are fits of eq 8 without the reaction term (only triplet term) to the experimental curves, and black heavy lines are fits of the complete eq 16 including the reaction term. The experimental curves were normalized at 0.01 ms and stacked to separate the different samples visually. The full curves and their fits extend up to 10 ms, but only the part at short correlation times is shown for clarity. The curves measured at the lowest excitation power in the presence of surfactant have been omitted for the sake of clarity. (b) Residuals plot corresponding to the fits shown in part a for TX-100 with one (gray lines) and two (black lines) bunching terms at 300 μW (dotted curve) and 740 μW (solid curve). (c) Residuals plot as in part b for Brij 35. The residuals are not weighted. The residuals from the fits to R123 in water have been omitted for clarity.

FCS Curves. Two different types of series of FCS correlation curves were measured: power series with varying excitation power at certain surfactant concentrations and titration series at constant excitation power and varying concentrations of surfactant. Increasing the excitation power leads to a higher population of the triplet state, so the influence of the triplet reaction term can be studied. This information allows one to choose a suitable excitation power for the titrations, where the entry/exit rate constants can be determined.

Figure 3 shows some of the FCS curves obtained at different excitation powers for R123 in aqueous solution, R123 in 31 mM TX-100 solution ([M] = 0.21 mM, ratio bound/free R123 = 14), and R123 in 21 mM Brij 35 solution ([M] = 0.52 mM, ratio bound/free R123 = 9.4). All curves show three regions: a fast increase in the range from 1 to 10 ns, followed by a slow decrease up to 10 μs, and a strong decrease down to 0 at longer times, which correspond to the antibunching, bunching, and diffusion terms, respectively, as described previously. In the intermediate bunching region, two processes may contribute: the triplet-state formation and the binding reaction ("reaction term"). The triplet-state population depends directly on the excitation power.[29,33] On the contrary, the reaction term does

not depend on excitation power but changes with the concentration of micelles (see eqs 14 and 15). Nevertheless, the triplet time and its amplitude could change for R123 bound to the micelles, making it difficult to distinguish the two types of bunching terms. This cannot be done visually, and therefore, a detailed analysis of the power-dependent FCS curves must be performed to establish whether a reaction term is present and whether the triplet term changes with the entrance of R123 into the micelles.

Beginning with free R123, the three FCS curves measured at different excitation powers can be satisfactorily fitted using eq 8 without the reaction term (Figure 3). A global fit of these three curves yields a triplet time τ_T of 1.8 ± 0.1 μs for R123 in aqueous solution, whose amplitude increases with the excitation power. At high concentrations of micelles, for both TX-100 and Brij 35, the FCS curves cannot be fitted with only one bunching term, as indicated by the systematic deviations of the fitted curves from the experimental correlation curves (see gray lines in Figure 3). Thus, it is necessary to introduce a second bunching term, the reaction term, to account for the variations observed in the microsecond region of the FCS curves in the presence of surfactant. Global fits of the curves for each surfactant at the highest micelle concentration (at which most dye is bound to micelles) using eq 16 with separated triplet and reaction terms are very satisfactory (see black lines in Figure 3) and yield triplet times of 4.0 ± 0.4 and 3.0 ± 0.4 μs for the R123 bound to TX-100 and Brij 35 micelles, respectively, which are longer than that of free R123.

The amplitudes of these terms increase with the excitation power as expected, but they are lower than the corresponding triplet amplitudes of free R123. Therefore, the triplet term contributes with longer times but smaller amplitudes in micelle-bound R123 than in free R123. The fits of these curves yield also reasonable values for the reaction times in the two surfactants, which are within error independent of the excitation power. More precise values will be obtained from the titration series. Taking into account these results, we conclude that the two terms are not strongly coupled and that the description of these two processes by the product of the corresponding terms, as in eq 16, is justified, especially at low excitation power.

The titration series of FCS curves measured for R123 in the presence of different concentrations of TX-100, from 0.02 to 10.8 mM, are shown in Figure 4. Similar curves were obtained for R123 with Brij 35 at concentrations varying from 0.04 to 20.6 mM. Both series were measured at very low excitation power ($\sim$62 μW) to minimize the contribution of the triplet state. For each surfactant concentration the corresponding micelle concentration was calculated using eq 1 and used for the fit. The three regions mentioned above are present in all of these curves: fast increase at short times due to excitation/deactivation from the single excited state (antibunching term), slow decrease in the microsecond time range due to both the triplet-state formation/deactivation and the reaction term (bunching terms), and decrease at times longer than 10 μs due to the diffusion of the molecule (diffusion term).

The first effect of the partition equilibrium is observed in the diffusion terms, as shown by the great increase of the diffusion times in the millisecond time range (inflection points of the diffusion terms) when increasing the surfactant concentration above the CMC (small gray vertical bars above τ_D in Figure 4). This must be attributed to the increasing amount of R123 molecules, which are bound to the micelles, and therefore diffuse much slower than R123 free in aqueous solution. In accordance with this interpretation, at concentrations of surfactant below

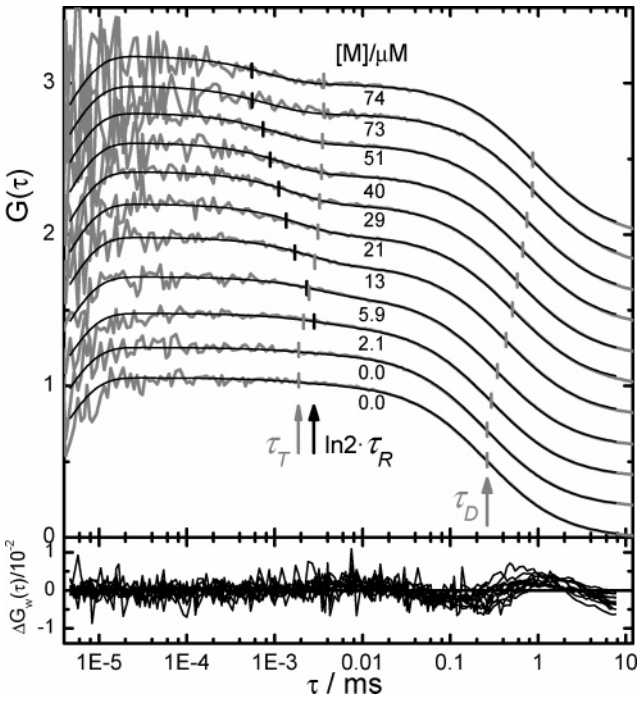

Figure 4. Upper panel: Correlation curves of R123 in aqueous solution (lowest gray line) and in the presence of different concentrations of TX-100 (upper gray lines), measured at a constant excitation power of 62 μW. Black curves are obtained by a global target fit of eq 16 to the experimental data. The triplet times of free and bound R123 were fixed at the known values as well as the binding equilibrium constant and the brightness known from bulk measurements (Table 1). The curves were stacked to separate them visually. The small vertical lines indicate the different decay times of the correlation functions determined from the fits as a function of the micellar concentration: mean diffusion time τ_D (gray), mean triplet time τ_T (gray), and reaction time τ_R (black), the latter indicated as half-life (τ_R ln2) of the reaction term. The lowest two curves were measured at surfactant concentrations much below the CMC (0.26 mM) at [S] = 0.022 mM and [S] = 0.053 mM, respectiveley. The lower panel shows weighted residuals. The weighting amplifies the residuals at long correlation times.

the CMC, where no micelles are present, the diffusion time is independent of the surfactant concentration and coincides with that determined in the absence of surfactant. As explained previously (eqs 11−13), a single diffusion term is observed in spite of the contribution of two species (free and micelle-bound R123), since the entry/exit dynamics are very fast compared to the diffusion rates. Thus, the observed diffusion time is a function of the concentration of micelles and of the diffusion times of free R123 (τ_f) and micelle-bound R123 (τ_b) as given by eq 13. These two diffusion times can be directly fitted in eq 16.

Partition of R123 between the aqueous phase and the micellar pseudo-phase has also an important effect on the bunching region of the concentration-dependent FCS curves (Figure 4), although this is not so easy to appreciate visually. As shown above, a reaction term that is dependent on micelle concentration appears at surfactant concentrations above the CMC in addition to the triplet term. Since the triplet times of free and bound R123 are different, as obtained from the analysis of the power-dependent correlation curves (Figure 3), the observed triplet time and triplet amplitude are expected to be weighted averages of those of free and bound R123 and can be calculated using a relation analogous to eq 17. Thus, the triplet times of free and bound R123 were fixed at the known values as well as the binding equilibrium constant and the brightness known from bulk measurements (Table 1). This fit strategy avoids correlation

TABLE 2: Results from Global "Target" Fits of Eq 16 to the Series of Correlation Curves Measured with Varying Surfactant Concentrations and Constant Excitation Power (62 μW)[a]

	τ_f/ms	τ_b/ms	$k_-/10^5$ s^{-1}	$k_+/10^{10}$ M^{-1}s^{-1}
R123 + TX−100 micelles	0.263 ± 0.002	1.66 ± 0.05	2.2 ± 0.1	1.4 ± 0.1
R123 + Brij 35 micelles	0.257 ± 0.003	2.4 ± 0.1	4 ± 1	0.8 ± 0.2

[a] During the fit the binding constants and the brightness ratios were fixed at the values given in Table 1. Antibunching times, triplet times, and triplet amplitudes were allowed to change with micelle concentration following the partition equilibrium (see text).

TABLE 3: Diffusion Coefficients, Hydrodynamic Radii, and Diffusion-Controlled Rate Constants Calculated from the Diffusion Times Given in Table 2 and Eqs 7, 19, and 20

	$D/10^{-10}$ m^{2}s^{-1}	R_h/Å	$k_d/10^{10}$ M^{-1} s^{-1}
R123 in water	3.5 ± 0.2	7.0 ± 0.4	
R123 bound to TX−100 micelles	0.57 ± 0.04	42 ± 3	1.5 ± 0.1
R123 bound to Brij 35 micelles	0.37 ± 0.03	67 ± 5	2.1 ± 0.2
TX−100 micelles	0.54[a]	45[a]	1.5[c]
Brij 35 micelles	0.54[b]	44[b]	1.5[c]

[a] Reference values from dynamic light scattering experiments without R123 from ref 15. [b] Reference values from dynamic light scattering experiments without R123 from refs 16, 18, and 19. [c] Calculated for diffusion between micelle and R123 using the reference values for D and R_h. All values are given for 25 °C. Uncertainties do not include calibration errors.

among the different fit parameters defined in the bunching region and leads to more precise values of the exit rate constant, which is our main interest. Nevertheless, in the case of Brij 35 the parameter correlation was still high and led to great uncertainties of the fitted parameters. As shown above, no coupling between the triplet term and the reaction term must be considered, especially at the low excitation power used for these measurements, at which the triplet-state population is very low (less than 3%).

Finally, the antibunching time can also be considered as a weighted average of free R123 and bound R123 times, and it was again calculated using eq 17. These two times, which practically coincide with the fluorescence lifetimes, were treated as free fit parameters.

Using eq 16 and following the strategy described above, global "target" analysis of the series of FCS curves with varying surfactant concentrations was performed. The fits were very satisfactory, as shown by the accordance of the fitted curves with the experimental data and the randomly distributed residuals (Figure 4). It must be noted that the empirical weighting function strongly amplifies the deviations in the diffusion region of the FCS curves. The remaining, very small systematic residuals in this region could be due to adsorption of the dye or to deviation of the sample geometry from the Gaussian profile. The main results of the fits are shown in Table 2. The entry rate constant k_+ is not a direct fit parameter, but it is calculated from the binding equilibrium constant K and the exit rate constant k_- (eq 9).

Diffusional Dynamics. Our analysis of the diffusion part at the slow end of the fluorescence correlation curves will focus on the diffusional dynamics of free and bound R123. Nevertheless, typical surfactant properties such as CMC and mean aggregation number could be also estimated from this type of data. The experimental diffusion times (marked inflection points in Figure 4) are constant at surfactant concentrations lower than the CMC and increase at higher concentrations, so the CMC could be estimated as the surfactant concentration at which the diffusion time starts to differ significantly from that of free R123. Note that this way to determine the CMC is more appropriate for weakly binding probes presenting a partition equilibrium than the method recently proposed by Zettl et al. for strongly bound probe−micelle systems of opposite charges, and it would probably explain the data obtained by these authors with nonionic surfactants and surfactants of the same charge as the probe.[14] An estimation of the mean aggregation number can be obtained from the hydrodynamic radius of the micelles (see below), assuming spherical particles.[11] However, the value of the mean density of the micelle is the main uncertainty in this calculation.

The diffusion times obtained from the analysis of the fluorescence correlation curves (Table 2) are converted to diffusion coefficients using eq 7 and then to the corresponding hydrodynamic radii R_h applying the Stokes−Einstein relation

$$R_h = \frac{kT}{6\pi\eta D} \tag{19}$$

where k is the Boltzmann constant and η the viscosity of water (0.8905 cP at 25 °C). The values obtained are given in Table 3.

The diffusion coefficient of free R123 coincides well with the value reported for the similar rhodamine 110 and pyronine B, another xanthene dye with approximately the same molar mass as R123.[3] It follows perfectly the power law dependence on molar mass determined for other charged rhodamines and pyronines in our previous work with an exponent of 0.7 that does not correspond to a spherical mass distribution but to a more planar conformation.[3]

In comparison with free R123, the diffusion coefficients of bound R123 are much lower. The value obtained for R123 bound to TX-100 micelles agrees perfectly with the literature diffusion coefficient of empty TX-100 micelles determined by dynamic light scattering.[15] (Values from some other references are significantly lower, but they are not based on such a detailed study as in the reference cited.) This indicates that the determined value of the diffusion coefficient reflects the translational motion of the micelles and that the presence of the small, noncovalently bound dye has no significant effect on the hydrodynamic properties of the micelle, unlike large fluorescent probes that perturb the micellar structure and lead to a significant decrease of the diffusion constant.[11] These results demonstrate again the great potential of FCS to determine diffusional properties of supramolecular structures.

In the case of Brij 35 micelles, the measured diffusion coefficient is significantly lower than that of TX-100 micelles, corresponding to a larger size, in spite of the much lower aggregation number of the Brij 35 micelles. However, the value obtained does not agree with the reported diffusion coefficient of Brij 35 micelles as determined with dynamic light scattering.[16] It is not reasonable to assume that R123 would have such a huge effect on the size of Brij 35 micelles, since that is not the

case for TX-100 micelles. A possible explanation for this disagreement may be the strong concentration dependence of both the aggregation number and the shape of Brij 35 micelles, studied in detail by Preu and co-workers.[18] The aggregation number increases by approximately 20% for a surfactant concentration of 10 mM as compared to the value near the CMC, and the micelles become ellipsoidal instead of spherical. Since the binding constant of R123 to Brij 35 micelles is not very large, relatively high concentrations of the surfactant must be used to obtain considerable amounts of bound R123. Therefore, the asymptotic value of the diffusion time of bound R123 may reflect the larger sizes and different shapes of Brij 35 micelles at high surfactant concentrations. This effect is not observed in TX-100 micelles since this surfactant shows much lower concentration dependence of the micellar properties.[15] A second hypothesis to consider is the existence of micelle fusion processes, which are strongly dependent on micelle concentration.[34]

Partition Dynamics. Now we will discuss the results regarding the dynamics involved in the partition equilibrium of R123 between the micellar pseudo-phase and the aqueous phase. Table 2 gives the values of the rate constants of dye entry (k_+) and exit (k_-) obtained from the fits of the fluorescence correlation curves. Note that the rate at which the rhodamine molecules enter into the micelles is the product of k_+ and the concentration of the micelles, which is for all studied concentrations much lower than the fluorescence deactivation rate of R123. Also the exit rate cannot compete with the deactivation rate of bound R123. This confirms that neither the association process nor the dissociation take place during the lifetime of the excited state.

The high values obtained for the entry rate constant suggest a diffusion-controlled process. The rate constants corresponding to a purely diffusion-controlled association process between R123 and the micelles can be estimated applying the Smoluchowski equation

$$k_d = 4\pi D_{DM} R_{DM} N_0 \tag{20}$$

where D_{DM} and R_{DM} are the sums of diffusion coefficients and hydrodynamic radii of the dye (free R123) and the micelles (bound R123), respectively, and N_0 is Avogadro's constant. Those properties have been obtained in the study of the diffusional dynamics (Table 3). The estimations of the diffusion-controlled rate constants are given in Table 3 using our data and the literature values. Comparing the values of k_+ (Table 2) with those of k_d, a perfect agreement in the case of TX-100 is found, which clearly indicates a diffusion-controlled entry rate constant. For Brij 35 micelles a smaller entry rate constant is obtained, which is approximately one-half of the diffusion-controlled values determined from our data or with values from the literature. Taking into account the great uncertainties implicit in the two rate constants, especially in the case of Brij 35, it is concluded that also in this case the association process is nearly diffusion-controlled, although not as clearly as in the case of TX-100. It must be noted that the entry rate constants found in this study are of the same order of magnitude as those reported for other molecules in different types of micelles, as determined by fluorescence quenching experiments.[4,5]

In a previous work on the association dynamics with cyclodextrins, representing molecular rigid cages, we found that the observed association rate constant was much lower than the diffusion-controlled rate constant.[3] This suggested that the association process follows a two-step mechanism: first the diffusion-limited formation of an encounter complex and then the inclusion reaction, which is determined by geometric and orientational requirements and is the rate-limiting step. In comparison to cyclodextrins, the studied micelles, especially the TX-100 micelles, behave as dynamic soft cages with no geometric or steric hindrances for the entrance of the dye, so every collision between dye and micelle leads to an effective association, and the entry rate constant is limited only by the diffusion rate of the molecules together.

The exit rate constants of R123 from the micelles to the aqueous phase are on the order of 10^5 s^{-1}, coinciding in magnitude with the dissociation rates found for the pyronine−cyclodextrin complexes.[3] As observed in that case, the different stability of the binding is mainly determined by the exit rates. The exit rate constant for R123 bound to Brij 35 micelles is a factor 2 higher than that for TX-100 micelles, contributing significantly to the difference observed between the corresponding binding constants (Table 1). Again, this factor is strongly influenced by the large uncertainty in the values obtained for Brij 35 micelles. As in the case of the cyclodextrin, the exit rate constant reflects the magnitude of the specific interactions responsible for the binding. Comparing the two systems under study, the interaction of R123 with TX-100 micelles is stronger than with Brij 35 micelles, in spite of the very similar structure of the two surfactants as poly(ethylene glycols). (Note that although the cores of the two types of micelles are significantly different it seems reasonable to assume that the charged R123 molecule locates at the hydrophilic shell.) A possible explanation may be the different mean densities of the two micelles, which would have an effect on the distances between the rhodamine and the poly(ethylene glycol) chains and thus on the interaction strength. Assuming spherical micelles of radius R_h, the mean density of the micelles can be estimated as follows

$$\text{density} = \frac{3N_{ag}M_S}{4\pi R_h{}^3 N_0} \tag{21}$$

with M_S being the molar mass of the surfactant. Using the same hydrodynamic radii for TX-100 and Brij 35 micelles, the mean density of the micelles increases with the aggregation number, resulting in a value 2 times higher for TX-100 micelles than that of Brij 35 micelles. This ratio even increases if a larger radius is considered for Brij 35 micelles. This might explain the higher exit rate constant observed for the less dense Brij 35 micelles. Note that the frequent use of eq 21 for the determination of aggregation numbers measuring hydrodynamic radii and assuming a typical micelle density may be very misleading.

MFD Diagrams. MFD measurements were performed for solutions of different concentrations of Brij 35 and with a R123 concentration at the single-molecule level. Figure 5 shows the two-dimensional (2D) histograms obtained after MFD analysis, where height represents the number of fluorescence bursts with a given anisotropy and fluorescence lifetime. The first histogram (Figure 5a) corresponds to a concentration of Brij 35 below the CMC, so no micelles are present. It is very similar to that obtained for R123 in the absence of surfactant. A single spot is observed in those diagrams corresponding to fluorescence bursts from free R123. Fitted Gaussian distributions yield mean values for the anisotropy and the fluorescence lifetime that are identical to those of R123 in the absence of surfactant (Table 4) and in perfect accordance to the values obtained in bulk measurements (Table 1). This confirms that these photophysical properties of R123 are not influenced by the presence of surfactant monomers.

When examining the 2D histograms for increasing concentrations of Brij 35 above the CMC (Figures 5b−5d), still only

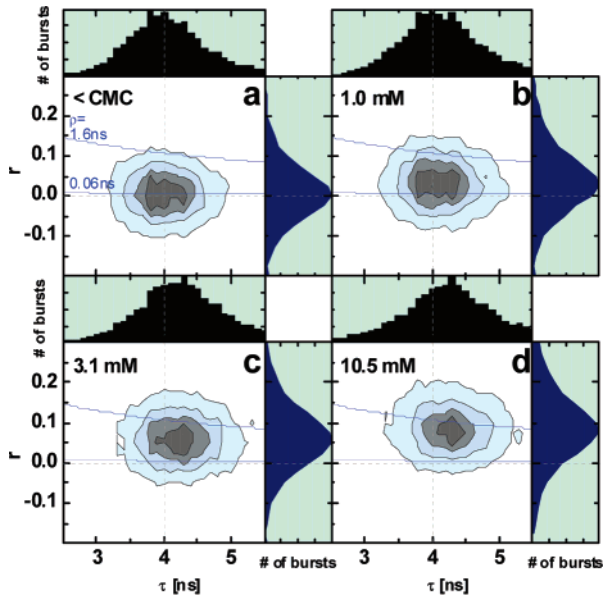

Figure 5. Two-dimensional burst number histograms of anisotropy, r, versus fluorescence lifetime, τ, obtained from MFD analysis of single-molecule measurements of R123 with different concentrations of Brij 35: (a) 0.042 mM (below CMC), (b) 1.0 mM, (c) 3.1 mM, (d) 10.5 mM. Blue lines represent values from Perrin's equation computed for two rotational correlation times ($\rho = 0.06$ ns and 1.6 ns).

TABLE 4: Mean Values and Widths (fwhm) of Anisotropy and Mean Fluorescence Lifetime Calculated by Fitting Gaussian Distributions to the Histograms Obtained from MFD Measurements

[Brij 35]/mM	mean τ /ns	width τ /ns	mean r	width r
0	4.0	0.87	0.005	0.11
0.042 (<CMC)	4.0	1.1	0.007	0.13
1.0	4.1	1.1	0.03	0.14
3.1	4.2	1.2	0.06	0.14
10.5	4.3	1.3	0.09	0.15
limit for totally bound R123[a]	4.3		0.11	

[a] Fitted mean values corresponding to a Brij 35 concentration at which R123 is totally bound to the micelles (see text).

one spot is observed and not two as might be expected, one for each of the species present, free R123 and R123 bound to the micelles. This demonstrates, in accordance to the FCS results, that the dye-exchange dynamics between free and bound R123 are faster than the typical duration of a fluorescence burst of some milliseconds. Due to the fast microsecond relaxation rates of the dye exchange, a R123 molecule changes during its transit through the detection volume many times between free and bound states. The lifetime and anisotropy determined from the photons of the burst appear therefore as averaged values of the lifetimes and anisotropies of free and bound R123.[35] It is also observed that the spot moves to longer lifetimes and higher anisotropy values as the surfactant concentration is increased. This is in agreement with the results of bulk measurements. The lifetime of R123 bound to Brij 35 micelles is slightly longer than that of free R123 (Table 1), so the mean fluorescence lifetime observed in MFD measurements will increase as the proportion of bound R123 increases. The same effect is observed if the bulk fluorescence decays are analyzed as single exponentials. Also steady-state anisotropy measurements showed that the anisotropy of bound R123 is higher than that of free R123 (Table 1) and that a weighted mean value is observed depending on micelle concentration. Moreover, it can be seen that the spot in the 2D histograms moves from a curve representing Perrin's equation with the rotational correlation time of free R123 ($\rho = 0.06$ ns, see above) to that calculated with the rotational correlation time of bound R123 ($\rho = 1.6$ ns) (Figure 5). This demonstrates the consistency of results between bulk measurements and single-molecule experiments.

Table 4 shows mean values and widths obtained for the one-dimensional histograms of fluorescence lifetime and anisotropy of MFD data assuming single Gaussian distributions. The mean values quantify the observed tendency of these properties to increase with the micelle concentration. The fits of a binding equilibrium model (eq 17 for lifetime and eq 18 for anisotropy) to these data are satisfactory and confirm the value of the binding constant. The fits yield also asymptotic values for τ and r of bound R123 (Table 4), which are in reasonable agreement with those obtained in bulk measurements (Table 1), taking into account the large uncertainties in the MFD values obtained from these Brij 35 samples.

The width of the distribution (Table 4) of pure dye in water is determined by the shot noise in the photon counting.[35] On the contrary, it is clearly observed that the distributions become slightly broader as the surfactant concentration is increased (Table 4). This broadening cannot be attributed to the presence of the fast interconverting species, free and bound R123, as their exchange rate is much faster than the typical burst duration, as determined by FCS. In all distributions it can be observed that the central part remains essentially symmetric, and an additional low but broad background is added (Figure 5). This is already observed at concentrations of Brij 35 lower than the CMC, at which no micelles are present, indicating that the Brij 35 impurities might be responsible for the observed broadening. However, other effects might also contribute: different binding sites, structure heterogeneity, micelle fusion, and surfactant polydispersity. Beside the dye exchange with a main population of binding sites observed in FCS data, at the single-molecule level the exchange with other minor populations of binding sites within the micelles may become visible. As mentioned above, Brij 35 micelles undergo structural changes at higher concentrations, increasing the mean aggregation number and deviating from a spherical shape, which would lead to a higher heterogeneity in their structure.[18] Dye exchange due to micelle fusion[34] may also be observed as a minor contribution. And finally one has to take into account that the commercial surfactants used may be chemically polydisperse with slightly different lengths of the poly(ethylene glycol) chains. These effects may lead to broader distributions of the fluorescence properties at the single-molecule level but not necessarily to observable changes in the FCS curves. To detect unequivocally these additional processes further MFD measurements with pure and monodisperse surfactants are underway. We think that studies of these systems at the single-molecule level will offer the possibility to identify structural features and dynamic processes that are not visible in bulk measurements due to ensemble averaging. The recently introduced probability distribution analysis of MFD histograms should be very suitable to identify these dynamic processes and heterogeneities.[35]

Acknowledgment. M.N. and W.A.S. thank the Xunta de Galicia and the Ministerio de Educación y Ciencia for financial support (Projects CTQ2004-07683-C02-02, PGIDT05PXIC26202PN, and HA2005-0063). Funding of this research by the SFB 633 (Molecular Response after Electronic Excitation) is acknowledged. The authors thank Professor M. Mosquera for the help with steady-state anisotropy measurements and very helpful discussions.

References and Notes

(1) Chattopadhyay, A. *Fluorescence Spectroscpy, Imaging and Probes: New Tools in Chemical, Physical, and Life Sciences*; Kraayenhof, R., Visser, A. J. W. G., Gerritsen, H. C., Eds.; Springer: New York, 2002; pp 211−224.

(2) Turro, N. J. *Proc. Natl. Acad. Sci. U.S.A.* **2005**, *102* (31), 10766−10770.

(3) Al-Soufi, W.; Reija, B.; Novo, M.; Felekyan, S.; Kühnemuth, R.; Seidel, C. A. M. *J. Am. Chem. Soc.* **2005**, *127* (24), 8775−8784.

(4) Kalyanasundaram, K. *Photochemistry in Microheterogeneous Systems*; Academic Press: New York, 1987.

(5) Gehlen, M. H.; De Schryver, F. C. *Chem. Rev.* **1993**, *93*, 199−221.

(6) Felekyan, S.; Kühnemuth, R.; Kudryavtsev, V.; Sandhagen, C.; Becker, W.; Seidel, C. A. M. *Rev. Sci. Instrum.* **2005**, *76*, 083104.

(7) Kühnemuth, R.; Seidel, C. A. M. *Single Mol.* **2001**, *2* (4), 251−254.

(8) Eggeling, C.; Berger, S.; Brand, L.; Fries, J. R.; Schaffer, J.; Volkmer, A.; Seidel, C. A. M. *J. Biotechnol.* **2001**, *86* (3), 163−180.

(9) Rothwell, P. J.; Berger, S.; Kensch, O.; Felekyan, S.; Antonik, M.; Wohrl, B. M.; Restle, T.; Goody, R. S.; Seidel, C. A. M. *Proc. Natl. Acad. Sci. U.S.A.* **2003**, *100* (4), 1655−1660.

(10) Valeur, B. *Molecular Fluorescence: Principles and Applications*; Wiley-VCH: Weinheim, Germany, 2002.

(11) Hink, M. A.; Van Hoek, A.; Visser, A. J. W. G. *Langmuir* **1999**, *15* (4), 992−997.

(12) Humpolickova, J.; Prochazka, K.; Hof, M.; Tuzar, Z.; Spirkova, M. *Langmuir* **2003**, *19* (10), 4111−4119.

(13) Yu, L.; Tan, M.; Ho, B.; Ding, J. L.; Wohland, T. *Anal. Chim. Acta* **2006**, *556* (1), 216−225.

(14) Zettl, H.; Portnoy, Y.; Gottlieb, M.; Krausch, G. *J. Phys. Chem. B* **2005**, *109*, 13397−13401.

(15) Phillies, G. D. J.; Stott, J.; Ren, S. Z. *J. Phys. Chem.* **1993**, *97* (44), 11563−11568.

(16) Phillies, G. D. J.; Hunt, R. H.; Strang, K.; Sushkin, N. *Langmuir* **1995**, *11* (9), 3408−16.

(17) Phillies, G. D. J.; Yambert, J. E. *Langmuir* **1996**, *12* (14), 3431−3436.

(18) Preu, H.; Zradba, A.; Rast, S.; Kunz, W.; Hardy, E. H.; Zeidler, M. D. *Phys. Chem. Chem. Phys.* **1999**, *1* (14), 3321−3329.

(19) Tomsic, M.; Bester-Rogac, M.; Jamnik, A.; Kunz, W.; Touraud, D.; Bergmann, A.; Glatter, O. *J. Phys. Chem. B* **2004**, *108* (22), 7021−7032.

(20) Deumié, M.; El Baraka, M. *J. Photochem. Photobiol., A* **1993**, *74*, 255−266.

(21) Pal, P.; Zeng, H.; Durocher, G.; Girard, D.; Giasson, R.; Blanchard, L.; Gaboury, L.; Villeneuve, L. *J. Photochem. Photobiol., A* **1996**, *98* (1−2), 65−72.

(22) Eggeling, C.; Widengren, J.; Rigler, R.; Seidel, C. A. M. *Anal. Chem.* **1998**, *70* (13), 2651−2659.

(23) Widengren, J.; Kudryavtsev, V.; Antonik, M.; Berger, S.; Gerken, M.; Seidel, C. A. M. *Anal. Chem.* **2006**, *78* (6), 2039−2050.

(24) Brand, L.; Eggeling, C.; Zander, C.; Drexhage, K. H.; Seidel, C. A. M. *J. Phys. Chem. A* **1997**, *101* (24), 4313−4321.

(25) Schaffer, J.; Volkmer, A.; Eggeling, C.; Subramaniam, V.; Striker, G.; Seidel, C. A. M. *J. Phys. Chem. A* **1999**, *103* (3), 331−336.

(26) Al-Soufi, W.; Novo, M.; Mosquera, M. *Appl. Spectrosc.* **2001**, *55* (5), 630−636.

(27) Elson, E. L.; Magde, D. *Biopolymers* **1974**, *13* (1), 1−27.

(28) Krichevsky, O.; Bonnet, G. *Rep. Prog. Phys.* **2002**, *65*, 251−297.

(29) *Fluorescence Correlation Spectroscopy: Theory and Applications*; Rigler, R., Elson, E. S., Eds.; Springer Series in Chemical Physics 65; Springer-Verlag: Berlin, 2001.

(30) Bhattacharyya, K. *Acc. Chem. Res.* **2003**, *36* (2), 95−101.

(31) Visser, A. J. W. G.; Vos, K.; Van Hoek, A.; Santema, J. S. *J. Phys. Chem.* **1988**, *92* (3), 759−765.

(32) Maiti, N. C.; Krishna, M. M. G.; Britto, P. J.; Periasamy, N. *J. Phys. Chem. B* **1997**, *101* (51), 11051−11060.

(33) Widengren, J.; Rigler, R. *Bioimaging* **1996**, *4* (3), 149−157.

(34) Rharbi, Y.; Winnik, M. A. *Adv. Colloid Interface Sci.* **2001**, *89*, 25−46.

(35) Antonik, M.; Felekyan, S.; Gaiduk, A.; Seidel, C. A. M. *J. Phys. Chem. B* **2006**, *110* (13), 6970−6978.